Available online at www.sciencedirect.com
ScienceDirect
Journal of Nuclear Materials 357 (2006) 183–190
journal of nuclear materials
www.elsevier.com/locate/jnucmat

Preparation, characterization and thermodynamic stability of $Rh_3Te_2O_{10}$

R. Mishra [a], S.R. Bharadwaj [a], D. Das [a,*], Martin Valldor [b], Rainer Pöttgen [b]

[a] Applied Chemistry Division, Bhabha Atomic Research Centre, Trombay, Mumbai 400 085, India
[b] Institut für Anorganische und Analytische Chemie, Westfälische Wilhelms-Universität Münster, Corrensstr. 36, 48149 Münster, Germany

Received 16 December 2005; accepted 14 June 2006

Abstract

A new ternary compound $Rh_3Te_2O_{10}$ was synthesized by reacting Rh_2O_3 and TeO_2 under 1 bar oxygen at 950 K. The compound was characterized by TG-DTA, XRD, EDX and magnetic susceptability analyses. From the TG experiment, the formation reaction could be expressed as $6Rh_2O_3(s) + 8TeO_2(s) + 3O_2(g) = 4Rh_3Te_2O_{10}(s)$. $Rh_3Te_2O_{10}$ crystallizes with a rutile type structure, $a = 456.6(2)$, $c = 385.9(1)$ pm, space group $P4_2/mnm$ (No. 136). The thermodynamic stability of the compound was determined by measuring the vapor pressure of $TeO_2(g)$. The vapor pressure over the two-phase mixture of Rh_2O_3 and $Rh_3Te_2O_{10}$ is given by the relation $\ln p(TeO_2)/Pa\ (\pm 0.07) = -36138.9 \cdot T^{-1} + 35.3$, $915 \leqslant T/K \leqslant 985$. The Gibbs energy of formation of the compound derived using the above vapor pressure data can be expressed as $\Delta_f G°(Rh_3Te_2O_{10}, s)\ (\pm 7.0\ kJ\ mol^{-1}) = -1510.3 + 0.897\ T$, $915 \leqslant T/K \leqslant 985$.

1. Introduction

Identification and characterization of the chemical states of fission products is an important facet of fuel chemistry in nuclear technology. The knowledge of the chemical states and their thermochemistry is prerequisite in the analysis of the distribution of fission products inside fuel pin and the release behavior of the products to the environment under off-normal or accidental situations. A number of noble metals such as ruthenium, rhodium and palladium are formed in considerable amounts during the fission of ^{235}U and other fissile nuclides [1]. They remain alloyed in the irradiated fuel pins [2] of fast breeder reactors, pressurized heavy water reactors, and boiling water reactors in different phases: white inclusions (metallic precipitates containing Mo, Tc, Ru, Rh and Pd), palladium based intermetallic compounds such as Pd (Pu, In, Sn, Te)$_{3+x}$ and mixed phases containing Sn, Sb and Te and many other similar phases. Tellurium, which is generated in moderate amounts in the nuclear fission remains distributed in the metallic phases, and has the tendency to segregate as intermetallic compounds with the noble metals [3,4]. Generally, Rh and Te do not form their oxides/mixed oxides under the reduced oxygen pressure prevailing in the fuel pin but when

* Corresponding author. Tel.: +91 22 25595102; fax: +91 22 25505151.
E-mail address: dasd@barc.ernet.in (D. Das).

0022-3115/$ - see front matter © 2006 Elsevier B.V. All rights reserved.
doi:10.1016/j.jnucmat.2006.06.007

the fuel containment fails under increasing $|p(O_2)|$ (e.g., in failed LWR pins) they do have the possibility of forming the oxides. The thermodynamic knowledge of the possible ternary oxides of tellurium is important in the analysis of tellurium release into the environment under accidental conditions.

Recently, we have presented the results of our investigation on the Gibbs energy of formation of Rh–Te intermetallic compounds Rh_3Te_2 and $RhTe_{0.9}$ by employing the Knudsen effusion vapor pressure technique [5]. As an extension of this work, we studied the oxidation behavior of these intermetallic compounds to look for possible ternary compounds in the Rh–Te–O system. The study led us to synthesize and characterize a new compound $Rh_3Te_2O_{10}$ of the Rh–Te–O ternary system. Rh in the +4 oxidation state is usually exhibited in its complexes and also, in simple compounds with high-electronegative elements. RhO_2, the black colored oxide of Rh with the oxidation state of +4 and a rutile structure can be prepared only by oxidation of Rh_2O_3 at 973–1073 K under high pressure of O_2 [6–9]. RhO_2 decomposes to Rh_2O_3 at 950 and 1163 K under 1 and 10 bar O_2 pressures, respectively [6]. However, we observed that in the presence of TeO_2, Rh_2O_3 oxidized from Rh^{+3} to Rh^{+4} under 1 bar of O_2 above 950 K to form a new ternary compound $Rh_3Te_2O_{10}$.

Lazarev et al. have reported preparations and physicochemical investigations of rhodium tellurate and tungstate of the type Rh_2MO_6 [10]. Apart from this there is no report on the formation of any other Rh–Te–O based compound. In this paper, we present the synthesis, characterization and thermodynamic stability of this new compound.

2. Experimental

The title compound was synthesized by heating a thoroughly ground mixture of Rh_2O_3 (Johnson, Matthey&Co.) and TeO_2 (Aldrich) (molar ratio 3:4) in a platinum container at a heating rate of 5 K/min up to 950 K under oxygen atmosphere and holding the temperature for 48 h. The sample was homogenized by repeated intermediate grinding. The product was slowly cooled inside the furnace. The formation of the compound was monitored using a SETARAM simultaneous TG-DTA (Model 92-16.18) instrument. The mass gain and the exothermic characteristics of the reaction among Rh_2O_3, TeO_2 and O_2 were noted. High-temperature decomposition characteristic of the formed compound was also monitored by TG-DTA studies up to 1273 K. XRD and EDX analyses were used for phase characterization of the compound as well as the TG residue after the decomposition. Phase studies were also made on long-annealed (at 975 K) mixtures of the stoichiometric compound with excess solid TeO_2, and with excess of solid Rh_2O_3 in air.

The X-ray powder diffraction (XRD) data for the Rietveld refinement were collected on a STOE STADI/P powder diffractometer equipped with a mini-PSD detector. Rietveld calculations for the compound were made on the data obtained in about 100 h of measuring time. The prepared compound was seen under SEM for phase morphology and crystallite size distribution. SEM and EDX studies were made to confirm the phase homogeneity and the uniformity of Rh and Te contents.

Magnetization measurements were carried out on a super-conducting quantum interference device (SQUID) magnetometer (Quantum Design: MPMS-5) in the temperature range 1.8–100 K in magnetic field strengths of 159.15, 238.73 and 397.9 kA/m. The magnetization hysteresis plot for the sample was recorded at 5 K in the field range ±5 T.

The thermodynamic stability of $Rh_3Te_2O_{10}$ was determined by measuring the partial pressure of $TeO_2(g)$ over the biphasic mixture of Rh_2O_3 and $Rh_3Te_2O_{10}$ in the temperature range 915–985 K using the Knudsen effusion technique. In the present measurement two solid phases co-existing with each other are in equilibrium with the vapor phase. Therefore, the measured pressure is uniquely defined as the degrees of freedom at a constant temperature are zero. The vapor pressure data $TeO_2(g)$ were generated by monitoring the effusing mass loss of the sample with the help of a thermobalance (SETARAM, Model B24). Detailed description of the apparatus and the procedure for the data collection are described elsewhere [5].

The mass calibration of the microbalance was done by recording the mass change on putting the standard weights on one of the pans of the balance at room temperature. The sample temperature calibration was done following the drop method [11], where the melting point of a high-pure metal hooked in thin strip form at the sample position in a thermobalance is noted by observing sudden mass change due to detachment during melting under slow and programmed heating. High purity metals, i.e., In, Sn, Sb, Ag and Au as standards were used for this

purpose. The temperature of the sample was controlled using a microprocessor-based temperature programmer cum controller with an accuracy of ±0.5 K using a Pt, Pt–13%Rh thermocouple. A Pt, Pt–10%Rh thermocouple used for measuring the sample temperature was located about 1 mm away from the sample, but well within the isothermal zone. The Knudsen cell suspended from the thermobalance by a thin platinum wire was located inside a vertically held impervious recrystallized alumina tube (internal diameter 30 mm); its top end was coupled with the thermobalance chamber. The thermobalance was attached to a high-vacuum system. The effusion experiments were done under 10^{-8} bar vacuum in dynamic conditions.

About 300 mg powdered sample was put in a silica cup inside the Knudsen cell of 15 mm diameter and 15 mm height, having a circular orifice of 1 mm diameter. The Clausing factor was determined experimentally by measuring vapor pressures of Ag(s), TeO_2(s), $CdCl_2$(s) and comparing them with the respective vapor pressures reported in the literature. The mean Clausing factor was found to be 0.946. In order to ensure the quick equilibrium between sample and its vapor products, the mixture of $Rh_3Te_2O_{10} + Rh_2O_3$ was well spread in the crucible so that the ratio of the projected surface of the sample to the orifice is high (about 50). This ratio as such was an order of magnitude higher than that of the spherically shaped frozen liquid of the silver standard used in the determination of the Clausing factor. The sample area augmentation was made to tackle any kinetic impedance from the vaporization reaction. The vapor pressures were measured both in ascending and descending mode of temperatures to ensure the absence of kinetic impediments of the vapor generation inside the cell.

The mass loss from the Knudsen cell was monitored for the $Rh_3Te_2O_{10} + Rh_2O_3$ two-phase mixture at different temperatures. The observed reproducibility in the mass loss rate in each isothermal run in ascending or descending orders of temperature fixation confirms the absence of kinetic hindrance in the evaporative loss. Several measurements were carried out in the temperature range of 915–985 K over the two-phase region. The equilibrium vapor pressure of TeO_2, derived from mass loss data was used to calculate the thermodynamic stability of $Rh_3Te_2O_{10}$. The residues in the silica crucible were analyzed after the experiments by X-ray diffraction to confirm the presence of the coexisting phases in the respective cases.

3. Results

3.1. Thermal analysis

Fig. 1 gives the TG-DTA plot for the Rh_2O_3 and TeO_2 mixture in the molar ratio 3:4, heated at a rate of 5 K/min in 1 bar oxygen. A mixture containing 25.68 mg Rh_2O_3 and 21.53 mg TeO_2 gained mass corresponding to 1.619 mg of oxygen starting at 680 °C and stabilized around 750 °C. The mass gain was accompanied by a huge exothermic peak. The mass gain from the TG curve together with the observation that both the oxides are fully consumed during the mass gain process in oxygen corroborates to the formation of a ternary oxide with the empirical formula $Rh_3Te_2O_{10}$. A similar mass gain was also observed when the Rh_3Te_2 intermetallic was oxidized in oxygen atmosphere at 500 °C, where the intermetallic is seen to have negligible vaporization loss due to Te [5]. XRD data of the oxidized sample showed characteristic lines due to the compound but no lines due to TeO_2 and Rh_2O_3. Fig. 2 gives the decomposition pattern of the heated sample at a rate of 5 K/min under flowing argon and oxygen atmosphere. In argon atmosphere the compound started decomposing in a single step at 1083 K to give a residue of Rh_2O_3, whereas in oxygen atmosphere the TG profile with the compound exhibited three steps of mass losses at 1123 K, 1290 K and 1438 K, respectively. Considering the stoichiometry of the starting compound, the TG steps could be assigned to the formation of the products, Rh_2TeO_6(s), RhO_2(s) and Rh(s) in the respective order.

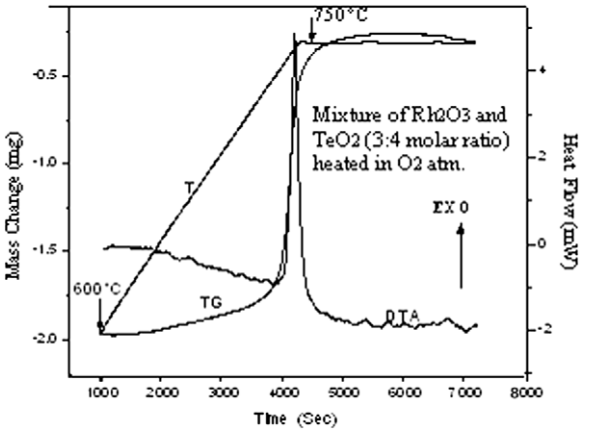

Fig. 1. TG-DTA plot for Rh_2O_3 and TeO_2 (3:4 molar mixture) heated at a rate 5 K/min under 1 bar oxygen.

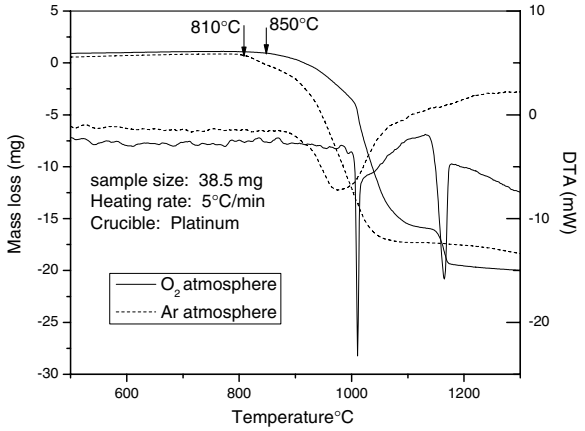

Fig. 2. Decomposition pattern of the compound heated at rate of 5 K/min under flowing argon atmosphere and oxygen.

3.2. XRD, and SEM/EDX studies

Fig. 3 gives the Rietveld refinement of the $Rh_3Te_2O_{10}$ crystal structure with the observed diffraction pattern (upper curve) and the difference between calculated and observed intensities (lower curve). The profile refinement of this phase shows good agreement with the observed profile as indicated by $R_{int} = 5.23\%$ and $R_p = 7.25\%$. The compound crystallizes in the rutile type structure with the cell parameters as $a = 456.6(2)$ pm, $c = 385.9(1)$ pm and space group $P4_2/mnm$ (No. 136). The atomic parameters are listed in Table 1. Fig. 4 gives the XRD patterns of $Rh_3Te_2O_{10}$, and 1:1 mixtures of $Rh_3Te_2O_{10} + Rh_2O_3$ and $Rh_3Te_2O_{10} + TeO_2$, respectively, after their annealing at 975 K for 100 h in air. The XRD plots show that the phases in the annealed mixtures remained intact with no change in their characteristic peak positions (Table 2). SEM/EDX measurements of the sample

Table 1
Atom co-ordinates in $Rh_3Te_2O_{10}$(s)

Atom	x	y	z	B (nm^2)	Occupancy
Te	0	0	0	0.016(2)	0.41
Rh	0	0	0	0.016(2)	0.59
O	0.302(5)	0.302(5)	0	0.006(7)	1.0

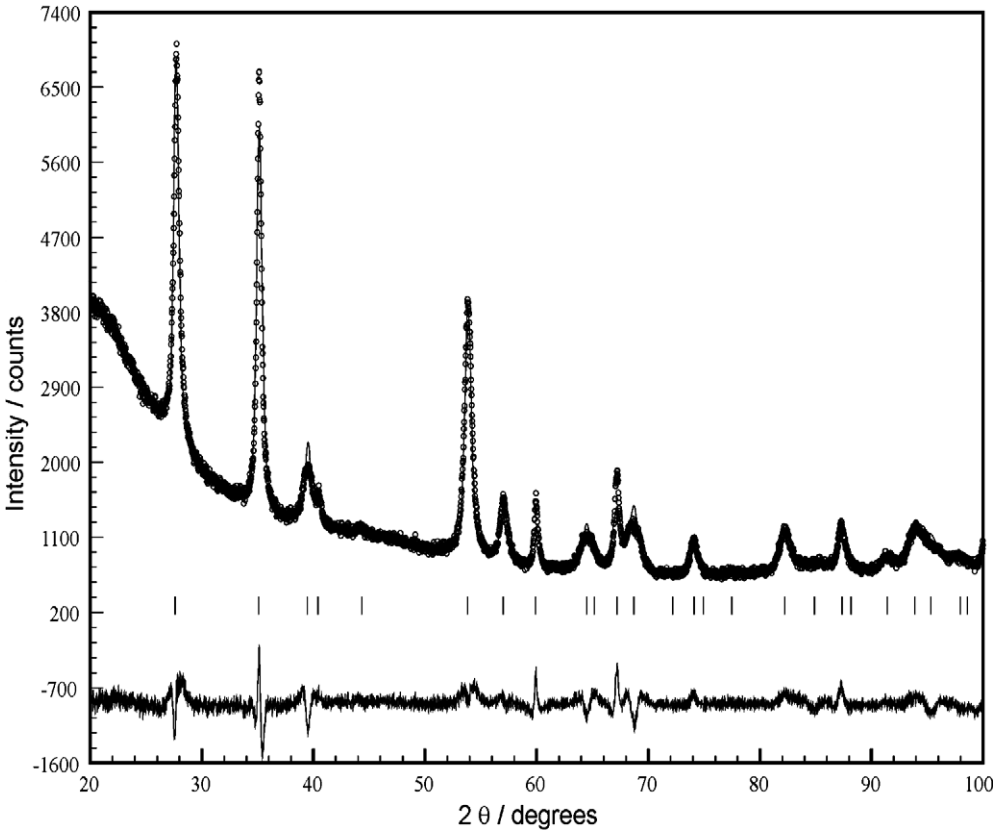

Fig. 3. Rietveld refinement of the $Rh_3Te_2O_{10}$ sample.

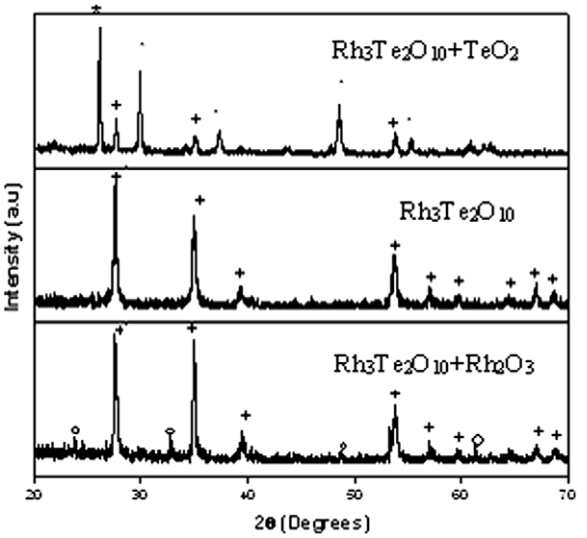

Fig. 4. XRD pattern of $Rh_3Te_2O_{10}$, $Rh_3Te_2O_{10} + Rh_2O_3$ and $Rh_3Te_2O_{10} + TeO_2$ annealed at 975 K for 100 h (+ = $Rh_3Te_2O_{10}$, ∗ = TeO_2 and ● = Rh_2O_3).

Table 2
Comparison of cell parameters of TeO_2, $Rh_{0.59(2)}Te_{0.41(2)}O_2$ and RhO_2

Compound	*a* (pm)	*c* (pm)
TeO_2	479	377
$Rh_{0.59(2)}Te_{0.41(2)}O_2$	456.6(2)	385.9(1)
RhO_2	449	309

taken at 10 different points resulted in the composition $Rh_{0.59(2)}Te_{0.41(2)}O_2$. The crystal sizes of the sample as observed from SEM were found to be within 1–5 μm.

3.3. Magnetic measurements

The magnetic susceptibility of the compound measured over a wide range of temperature from 1.8 to 300 K showed that the compound is paramagnetic in nature. This can be seen from the plot of specific susceptibility versus temperature (Curie behavior) at 397.9 kA/m (Fig. 5). Similar behavior was also seen for magnetic field strengths 159.15 and 238.73 kA/m, but it is not shown here. The corresponding Curie plot of $1/\chi$(g) vs. T for 397.9 kA/m field is shown in Fig. 6. The magnetic moment per Rh atom calculated from the slope of the above plot was found to be 0.46 μ_B. This corresponds to a spin value of about 0.05 indicating significant quenching in the spin of the unpaired electron of Rh^{+4}. This will be further discussed in Section 4. The hysteresis

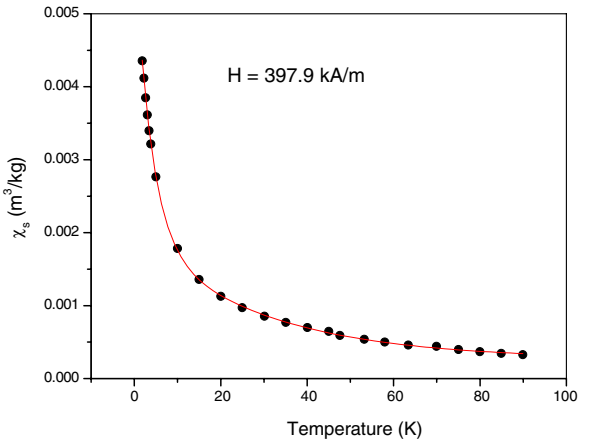

Fig. 5. Plot of the specific susceptibility of $Rh_3Te_2O_{10}$ vs. temperature at 397.9 kA/m.

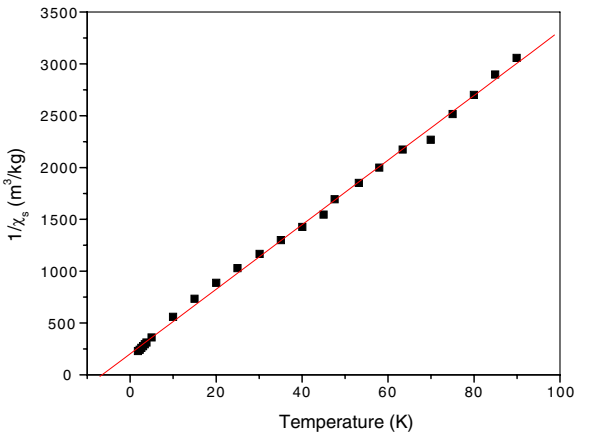

Fig. 6. Curie plot of $1/\chi$(g) of $Rh_3Te_2O_{10}$ vs. *T* at 397.9 kA/m.

curve for the compound measured at 5 K is shown in Fig. 7. The shape of the curve shows near absence of hysteresis in the compound.

3.4. Thermodynamic stability of $Rh_3Te_2O_{10}$

Thermogravimetric and differential thermal analysis (TG-DTA) plot (Fig. 2) showed that the compound $Rh_3Te_2O_{10}$ incongruently vaporizes at 1068 K in argon atmosphere to form Rh_2O_3(s) and TeO_2(g) in a single step. No break was seen in the TG plot for the decomposition of the compound. XRD data for the residue of partially decomposed $Rh_3Te_2O_{10}$ obtained from the Knudsen effusion studies showed the presence of lines due to Rh_2O_3 and $Rh_3Te_2O_{10}$ compounds only. On indexing the XRD lines of the Rh_2O_3 and $Rh_3Te_2O_{10}$

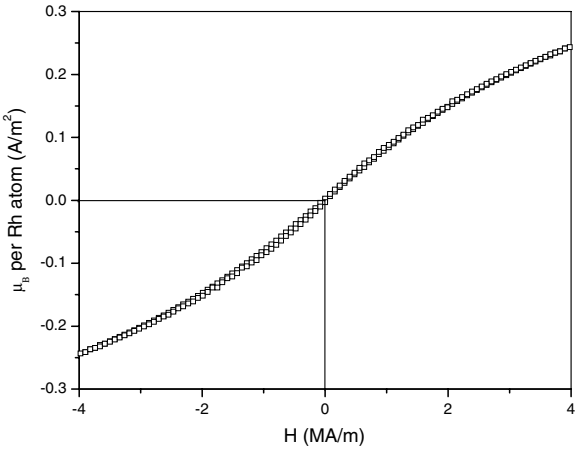

Fig. 7. Hysteresis curve of $Rh_3Te_2O_{10}$ measured at 5 K.

compounds, no change of the cell parameters could be observed as compared to the starting materials. This is indicative of the fact that the stoichiometry of the compound is retained after the reaction. It was observed from the available thermodynamic data [12] on tellurium dioxide, that $TeO_2(g)$ is the most predominant vapor species in the experimental range of temperature and the total pressure of tellurium bearing species (10^{-7} bar) as reflected in the mass loss rates. Therefore, the vaporization of $Rh_3Te_2O_{10}$ during the effusion process was considered through the following reaction path:

$$Rh_3Te_2O_{10}(s) = 3/2Rh_2O_3(s) + 2TeO_2(g) + 3/4O_2(g) \quad (1)$$

The isothermal rate of effusion of tellurium oxide vapors and $O_2(g)$ from the orifice was obtained from the observed total mass loss over a time t at steady state. The vapor pressure of tellurium bearing species $p(TeO_2)$, in the Knudsen cell was derived from the mass loss/time data using the relation of effusive flow obtainable from the kinetic theory of gases applied to vapor fluxes of the two species. The total mass loss m_T within time t consists of $m(TeO_2)$ and $m(O_2)$, which according to Eq. (1) corroborates to the molar ratio and therefore the flux ratio of 1:0.375, respectively. Therefore, $m_T \times M(TeO_2)/[M(TeO_2) + 0.375M(O_2)] = m(TeO_2)$, M = molecular weight. The following relation then expresses the vapor pressures of $TeO_2(g)$ in terms of the quantity $m(TeO_2)$:

$$p(TeO_2) = (1/A) \times 1/K_c \times [m(TeO_2)/t] \times [2\pi RT/M(TeO_2)]^{1/2} \quad (2)$$

Table 3
Vaporization data for the reaction $Rh_3Te_2O_{10}(s) = 3/2Rh_2O_3(s) + 2TeO_2(g) + 3/4O_2(g)$

Temperature T (K)	Time, t (s)	Mass loss, w (μg)	$p(TeO_2)$ (Pa)	$\Delta_f G^\circ$ (kJ/mol)
915.5	600	27	0.014	−133.42
927	600	51	0.026	−133.1
937	600	82	0.042	−132.78
949	600	134	0.069	−132.43
962	600	184	0.096	−132.33
973	600	294	0.154	−132.15
985	600	461	0.243	−131.90
979.5	600	393	0.207	−131.73
969	600	264	0.138	−131.69
958.5	600	179	0.093	−131.62

In Eq. (2), $p(TeO_2)$ is the vapor pressure of TeO_2, A the orifice area, K_c the Clausing factor, T the absolute temperature in Kelvin, $M(TeO_2)$ the molecular weight of TeO_2 species, R the universal gas constant.

The vapor pressure of $TeO_2(g)$ over the $Rh_3Te_2O_{10}(s)$ and $Rh_2O_3(s)$ mixture in the temperature range 915–985 K as calculated from experimentally determined parameters involved in Eq. (2) are given in Table 3 for all the runs. The linear least-square fit of $\ln p(TeO_2)$ versus $1/T$ is given in Fig. 8. The least-square fitted equation is represented as

$$\ln p(TeO_2)/Pa \pm 0.07 = -36138.3/T + 35.3 \quad (915 \leqslant T/K \leqslant 985) \quad (3)$$

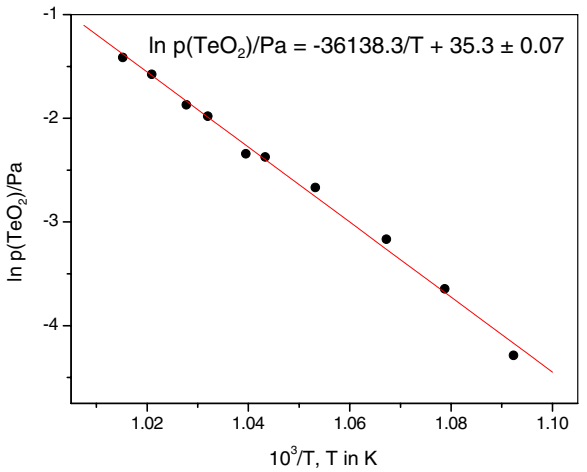

Fig. 8. Linear least-square fit of $\ln p(TeO_2)$ vs. $1/T$ for the incongruent vaporization of $Rh_3Te_2O_{10}$.

The slope and intercept of the linear equations yield the values of mean molar enthalpy and entropy, for TeO_2(g) vaporization according to reaction (1) over the working range of temperatures. These values of enthalpy and entropy are 300.7 kJ mol^{-1} and 197.6 J K^{-1} mol^{-1}, respectively.

3.5. Gibbs energy of formation of $Rh_3Te_2O_{10}$

The Gibbs energy of formation of $Rh_3Te_2O_{10}$ was derived using the above vapor pressure data. The XRD data of the partially decomposed sample after the vapor pressure study showed the lines of pure Rh_2O_3 and $Rh_3Te_2O_{10}$. Therefore, the Gibbs energy of formation of $Rh_3Te_2O_{10}$, was derived using Eq. (3) and reaction (1) according to the $Rh_3Te_2O_{10}$ phase co-existing with pure Rh_2O_3(s). Further, it was assumed that $Rh_3Te_2O_{10}$ has a very narrow homogeneity range.

Considering the decomposition reaction for the compound $Rh_3Te_2O_{10}$ (Eq. (1)) the equilibrium constant K can be given by the relation

$$K = p^2(\mathrm{TeO_2}) \times p^{3/4}(\mathrm{O_2}). \tag{4}$$

Taking the flux ratio 1:0.375 in the effusive flow of TeO_2(g) and O_2(g) it can be seen that $p(O_2) = 0.375 \times [M(O_2)/M(TeO_2)]^{0.5} \times p(TeO_2)$. Hence the Gibbs energy change for the vaporization reaction is expressed as

$$\begin{aligned}\Delta_r G^0 &= -RT \\ &\quad \times \ln\left[p^2(\mathrm{TeO_2})\left\{0.375 \times \left(\frac{M(\mathrm{O_2})}{M(\mathrm{TeO_2})}\right)^{1/2} p(\mathrm{TeO_2})\right\}^{3/4}\right] \\ &\equiv -RT \ln[p^{11/4}(\mathrm{TeO_2}\{0.1679\}^{3/4})]\end{aligned} \tag{5}$$

Using Eqs. (5) and (3), the Gibbs energy of formation of $Rh_3Te_2O_{10}$(s) can be expressed as

$$\begin{aligned}\Delta_f G^\circ(\mathrm{Rh_3Te_2O_{10}}) &= 3/2\Delta_f G^\circ(\mathrm{Rh_2O_3}) \\ &\quad + 2\Delta_f G^\circ(\mathrm{TeO_2, g}) \\ &\quad + RT \ln(p_{\mathrm{TeO2}}^{11/4} \times (0.1679)^{3/4})\end{aligned} \tag{6}$$

The values of the Gibbs energy of formation of pure Rh_2O_3(s) and TeO_2(g) were taken from Ref. [12]. The Gibbs energy of formation of $Rh_3Te_2O_{10}$(s) thus can be expressed by the equations

$$\begin{aligned}&\Delta_f G^\circ(\mathrm{Rh_3Te_2O_{10}, s})(\pm 7.0\ \mathrm{kJ\,mol^{-1}}) \\ &\quad = -1510.3 + 0.897 \cdot T \quad (915 \leqslant T/K \leqslant 985)\end{aligned} \tag{7}$$

Therefore, the average standard enthalpy and entropy of formation of $Rh_3Te_2O_{10}$ at the mean temperature of measurement 950 K are –(1510 ± 12) kJ mol^{-1} and –(897 ± 10) J K^{-1} mol^{-1}.

4. Discussion

The difference plot from the Rietveld refinement contains no residual peaks unless those accounted for. The broadness of the peaks could be due either to (i) small crystal sizes or (ii) to the fact that Rh and Te are involved in a solid solution, which is not perfectly ordered. With larger annealing time it was possible to get a product with larger crystals. The EDX analyses on such crystals did not show variations in Rh and Te composition, which somewhat sets aside case (ii). The cell parameters derived from the XRD data show that they do not exactly fall in line with the hypothesis of solid solution, $Rh_{0.59(2)}Te_{0.41(2)}O_2$, of the two oxides both of which having rutile structure. Whereas the derived parameter a fits nicely in between the two previously reported data of TeO_2 [9] and RhO_2 [6,13], the parameter c is seen to be larger even than that of TeO_2. Stacking faults need not lead to the higher mosaicity in c-direction than present in the RhO_2–TeO_2 lattices. Also from the XRD results of the long-annealed mixtures of $Rh_3Te_2O_{10} + Rh_2O_3$ and $Rh_3Te_2O_{10} + TeO_2$ in air, that the added binary oxide phase remained intact, the solid solution hypothesis is ruled out. Considering the fact that two tetravalent cations significantly differ in their crystal radii $r(Rh^{+4}) = 0.06$ nm and $r(Te^{+4}) = 0.097$ nm and in their electronegativities, ($\chi_{Rh} - \chi_O = -2.0$, and $\chi_{Te} - \chi_O = -1.5$), the observed higher mosaicity is rather indicative of compound formation.

From the magnetic susceptibility measurement data it was found that the compound has a magnetic moment of 0.46 μ_B per Rh atom. For the Rh^{+4} ion in its octahedral geometry (rutile structure), the number of unpaired electrons is one, which corresponds to a magnetic moment 1.73 μ_B. The reduction of the magnetic moment from 1.73 μ_B for pure RhO_2 (Rh^{+4}) to 0.46 μ_B in case of the compound suggests that the magnetic moment of the unpaired electron is significantly quenched in the compound. Quenching of the magnetic moment of the unpaired electron of the Rh^{+4} atom is suggestive of the involvement-bonding interaction. The bonding was further evident by estimating the stability of the compound relative to its constituent oxides,

namely RhO_2 and TeO_2 solids. Thus considering the standard Gibbs energy of formation of the compound as derived in Eq. (7) and also considering the reported Gibbs energy of formation data, for the constituent oxides, namely $\Delta_f G°(RhO_2,s)$ (kJ mol^{-1}) $= -239.0 + 0.178 \cdot T$ and $\Delta_f G°(TeO_2,s)$ (kJ mol^{-1}) $= -317.7 + 0.169 \cdot T$, one obtains the relative stability as $\Delta_f G°(Rh_3Te_2O_{10}, s)$ (kJ mol^{-1}) $= -157.9 + 0.026 \cdot T$, $(915 \leqslant T/K \leqslant 985)$. It shows that the dioxide attends an enthalpic stability of -157.9 kJ mol^{-1} and entropy ordering of 26 J K^{-1} mol^{-1} in the compound formation. The thermodynamic stability of the TeO_2 component in the compound is apparent from its low activity deducible from Eq. (3) in conjunction with the reported vapor pressure of TeO_2(g) as $\ln a(TeO_2) = -5690/T + 2.0$. Evidently, the TeO_2 activity is reduced by 40–50 times in the compound. It can be noted here that in the calculation of Gibbs energy of formation data, we have considered Rh_2O_3 as the co-existing phase and not Rh_2TeO_6, which should have been the co-existing phase as per literature [14]. The assumption of Rh_2O_3 as the co-existing phase is based on our experimental observation of the decomposition pattern and the XRD analysis of the partially decomposed products obtained under Knudsen evaporation. The observed difference in the TG results under argon and oxygen flow conditions (Fig. 2) led to the understanding that the reported Rh_2TeO_6 is the product phase of $Rh_3Te_2O_{10}$ according to $Rh_3Te_2O_{10}(s) = Rh_2TeO_6(s) + TeO_2(g)$ when carried out in oxygen environment. In order to understand the dependence of the product formation on $p(O_2)$, the mass loss rates in oxygen and in argon were compared at the same temperature and transpiration rate of the respective gases. Knowing that the mass loss in argon that took place according to reaction (1) and considering the measured values of $p(TeO_2)$ in the reaction, the $p(TeO_2)$ pressure of the $Rh_3Te_2O_{10}(s)$ decomposition in oxygen could be estimated as $\ln p(TeO_2)/Pa = -26937/T + 26.6$. The Gibbs energy of formation of Rh_2TeO_6 derived from the estimation can be given by $\Delta_f G°(Rh_2TeO_6, s)$ (kJ mol^{-1}) $= -910.7 + 0.642 \cdot T$. The result suggests that Rh_2TeO_6 would decompose to Rh_2O_3(s), TeO_2(g) and oxygen when $p(O_2)$ is below the value given by the relation $\ln p(O_2)/Pa = -38134/T + 43.5$. At 1000 K, for example, Rh_2TeO_6 should not decompose to form Rh_2O_3(s), TeO_2(g) and oxygen if $p(O_2)$ is higher than 2×10^{-3} bar. This explains why $Rh_3Te_2O_{10}$(s) follows the decomposition path $Rh_3Te_2O_{10}(s) = 3/2\ Rh_2O_3(s) + 2\ TeO_2(g) + 3/4\ O_2$ (g) under argon with an impurity of 10 ppm oxygen.

The above discussion on the results of crystallographic, magnetic, thermal and thermodynamic analyses leads to the fact that a compound of the stoichiometry $Rh_3Te_2O_{10}$ exists in the Rh–Te–O ternary.

5. Conclusion

A new ternary compound $Rh_3Te_2O_{10}$ belonging to the Rh–Te–O system is reported for the first time. The sample was characterized by TG-DTA, XRD, EDX and magnetic susceptibility measurements. The thermodynamic stability of the compound was determined by measuring the vapor pressure of TeO_2 over the two-phase mixture of Rh_2O_3 and $Rh_3Te_2O_{10}$.

Acknowledgement

The authors are thankful to Dr P.K. Mishra of Technical Physics and Prototype Division, BARC for magnetic susceptibility measurements.

References

[1] H. Kleykamp, J. Nucl. Mater. 131 (1985) 221.
[2] J.I. Bramman, R.M. Sharpe, D. Thom, G. Yates, J. Nucl. Mater. 25 (1968) 201.
[3] A.A. Men'kov, L.N. Komissarova, Yu.P. Simanov, V.I. Spitsyn, Dokl. Akad. Nauk SSSR 141 (1961) 3642.
[4] J.H. Brixner, J. Inorg. Nucl. Chem. 15 (1960) 199.
[5] R. Mishra, M. Ali, S.R. Bharadwaj, D. Das, J. Nucl. Mater. 321 (2003) 318.
[6] O. Muller, R. Roy, J. Less-Common Metals 16 (1968) 129.
[7] D.D. Beck, C.J. Carr, J. Catal. 144 (1993) 296.
[8] D.D. Beck, C.J. Carr, J. Catal. 144 (1993) 311.
[9] Z. Weng-Sieh, R. Gronky, A.T. Bell, J. Catal. 170 (1997) 62.
[10] V.B. Lazarev, I.I. Prosychev, I.S. Shaplygin, Russ. J. Inorg. Chem. 24 (1979) 173.
[11] O. Kubaschewski, C.B. Alcock, P.J. Spencer, Metallurgical Thermochemistry, sixth ed., Pergamon, Oxford, 1993.
[12] FACTSAGE™ 5.0. Thermochemical Software for Windows™, obtained from GTT Technologies, Germany, 2001.
[13] V.M. Goldschmidt, T. Barth, D. Holmsen, D. Lunde, W. Zachariasen, Skr. Nor. Vidensk Akad. Oslo 1 (1926) 5.
[14] R.D. Shannon, Solid State Comm. 6 (1968) 139.